A Haptic Mouse Design with Stiffening Muscle Layer for Simulating Guarding in Abdominal Palpation Training

Liang He[1,3], Florence Leong[1], Thilina Dulantha Lalitharatne[1], Simon de Lusignan[2], and Thrishantha Nanayakkara[1]

***Abstract*— A patient would contract surface muscles as a reaction called muscle guarding when experiencing discomfort and pain during physical palpation. This reaction carries important information about an affected location. Training physicians to regulate palpation forces to elicit just enough muscle tension is a challenge using real patients. Tunable stiffness mechanisms enabled by soft robotics can be effectively integrated into medical simulator designs for effective clinical education. In this paper, we propose a controllable stiffness muscle layer to simulate guarding for abdominal palpation training. Designs with soft, fine, and rigid granular jamming, stretchable and non-stretchable layer jamming mechanisms were tested and evaluated as methods to create controllable stiffness muscle. User studies have been carried out on 10 naive participants to differentiate the tense and relaxed abdomen with the proposed jamming mechanisms. Muscle samples made of ground coffee (fine granular jamming) and latex layers (stretchable layer jamming) show good usability in simulating abdomen with different stiffness with at least 75% of the user data exhibits more than 70% of decision accuracy for both tested palpation gestures (single finger and multiple fingers) after short pre-training.**

I. INTRODUCTION

Often primary examination of a patient by a general practitioner (GP) involves physical examination to estimate the condition of internal organs in the abdomen [1]. Abdominal palpation is one such method widely used by GPs to exclude an acute abdomen, for localized tenderness, or enlarged organs [2]. Haptic information such as tissue stiffness, organ texture, and visual perception through facial expressions are often used as feedback to test a range of medical hypotheses for diagnosis during the palpation examination of the abdomen [3]. Although well-established guidelines, protocols, and improvements in efficiency for the manual palpation examination methods are available, the effectiveness of techniques such as palpation depends on the skill of the GPs, which is often challenging to master and requires years of experience [4].

Differentiating voluntary tense from involuntary guarding when there may be peritoneal inflammation is an important part of clinical assessment [5], [1]. Voluntary muscle tensing is a voluntary contraction of the abdominal muscles during the examination and is often generalized over the entire abdomen [5]. Involuntary guarding, also known as rigidity or abdominal spasm, is an involuntary reflex contraction that transpires overlying tissue inflammation, which involves only the specific inflamed area. During the examination, the elicitation of tenderness is often indicated by a facial expression of pain [5], [6]. The associate techniques are difficult for novice examiners to master.

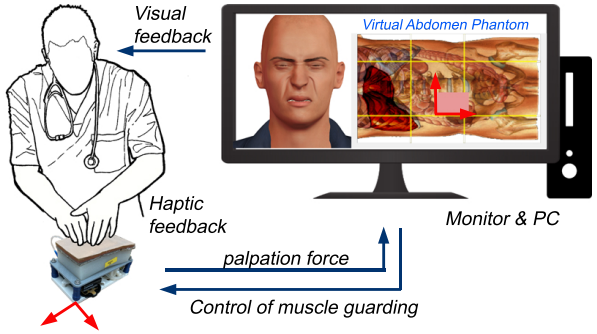

Fig. 1. The haptic mouse for virtual palpation training of abdominal muscle guarding with a configurable physical interface enabled by soft robotic jamming.

An abdominal phantom capable of simulating the above-mentioned abdominal muscle reactions for palpation training would provide an effective training scenario for medical trainees [7]. Furthermore, to emulate the muscle conditions, the abdominal phantom needs to provide haptic feedback to assist the training. An abdominal phantom for palpation training should consist of at least the major parts of the human abdomen, such as fat layers, muscle layers, and organs, to mimic the abdomen [8]. However, to design the abdominal muscle layer for palpation training, the key is to develop an approach that can simulate the stiffness change during muscle guarding [9].

Researchers have intensively studied tunable stiffness mechanisms in medical simulators' design to provide realistic haptic feedback in a simulated environment [10]. However, current haptic devices used with virtual reality training have limited interacting points [11]. With recent advancements in material science and soft robotics [12], a new category of simulators that can physically simulate both kinesthetic [13] and cutaneous feedback is emerging; namely, the configurable physical interface. This approach has the advantages of simulating a physical environment that can enable diverse contact models in contrast to the single contact

*This work was supported by the Engineering and Physical Sciences Research Council (EPSRC) RoboPatient grant EP/T00603X/1.

[1] L. He, F. Leong, T. Lalitharatne, and T. Nanayakkara are with the Dyson School of Design Engineering, Imperial College London, UK L.he17@imperial.ac.uk

[2] S. de Lusignan is with the Nuffield Department of Primary Care Health Sciences, University of Oxford, UK

[3] L. He is also with the Oxford Robotics Institute, University of Oxford, UK

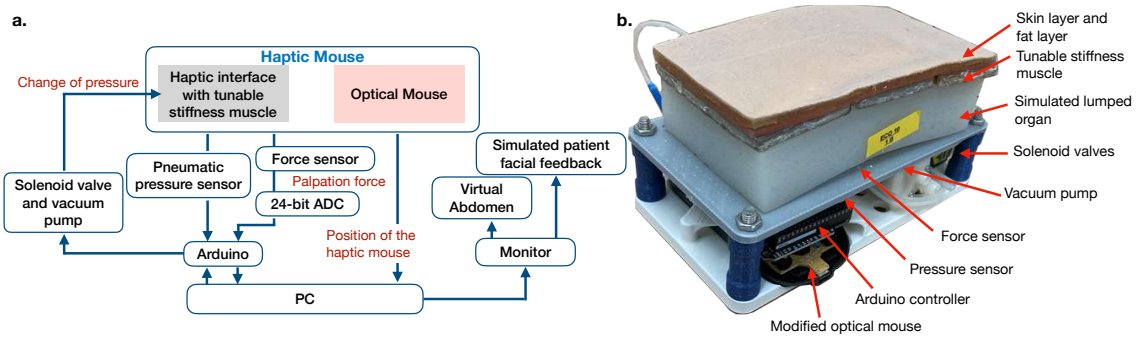

Fig. 2. **(a)** Proposed haptic mouse system diagram. **(b)** The hardware design of the haptic mouse.

in the conventional haptic device (e.g., Phantom devices from 3D Systems [14]). Granular jamming has been used to provide regional inclusion in recent interface design [15]. Stanley and Okamura [16] proposed a surface display that can change geometry by programming the pressure of the inflating layer and granular jamming stiffening layer. He et al. [17] implemented positive pressure granular jamming in simulating tunable stiffness liver tumors and used the nodules as soft sensors [18]. A similar granular jamming idea to create a configurable object with stiffness control can be found in [19], where a programmable soft 3D object is presented. However, the application of such a physical haptic interface in medical training is still in its infancy.

Thus, in this paper, we propose a method to simulate muscle guarding with a haptic interface driving by negative pressure jamming effect. The configurable physical interface is designed in the form of a haptic mouse, sensing the palpation force with a force/torque sensor and simulating contracted or relaxed muscle by applying or removing negative pressure on the designed muscle layer. This paper shows the first generation of a physical configurable interface in VR-based palpation training. The design and fabrication of the training system, configurable physical interface, and tunable-stiffness muscle layer are detailed in Section II and Section III. The proposed artificial muscle layers are experimentally characterized in comparison to a piece of ex-vivo porcine belly sample, shown in Section IV. Section V describes a user study that was carried out to evaluate and validate the proposed mechanisms through a series of palpation training tasks. The research findings and future directions are discussed and concluded in Section VI.

II. Haptic Mouse for Closed-Loop Virtual Palpation Training

The proposed training system consists of a haptic mouse, a virtual abdomen training model, and a facial expression unit (see Fig. 1). The haptic rendering is achieved via the haptic mouse, a phantom made of soft robotic jamming mechanisms (Fig. 2b). The visual abdomen model represents the relative virtual location of the haptic mouse to the synthesized patient abdomen, and the facial expression unit indicates the associated patient pain during palpation. The objective of the system is to train the detection of voluntary or involuntary

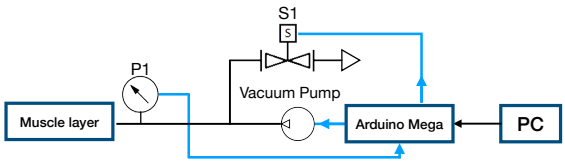

Fig. 3. Pneumatic system connections (P1 stands for the pressure sensor; S1 stands for solenoid valve).

guarding with pain expressions to show tenderness in a virtual environment. With the virtual patient displayed on a PC monitor, the trainee can replicate the palpation maneuvers on the abdomen of a real patient by manually moving the physical interface to explore a different part of the abdomen on the virtual patient, similar to moving a computer mouse.

The detailed system diagram can be found in Fig. 2a. A modified optical mouse measures the position of the physical setup, and the palpation force is simultaneously recorded by the underlying force sensor (2kg Miniature S-Beam Load Cell, APPLIED MEASUREMENTS LTD) via an HX711 24-Bit Analog-to-Digital Converter (ADC) (Avia Semiconductors). The haptic interface's position data are also processed with the program and mapped to the virtual abdomen. The algorithm incorporates the closed-loop control of the pain expression and the haptic interface stiffness via palpation force and position. Fig. 3 shows the pneumatic system used to change the vacuum pressure of the tunable stiffness muscle layer, include a small vacuum pump (12V), a solenoid valve (S1, VDW10AA, SMC), a pressure sensor (P1, $\pm$100kPa, PSE 543-R06, SMC Corporation, Japan), and an Arduino Mega 2560 microcontroller. During the simulation, the vacuum pump is set to be constantly on to suppress the effect on motor sound for different simulated conditions. During the non-guarding state, S1 is set to be open. When the algorithm detects the need to simulate muscle guarding, signals will be sent through the Arduino microcontroller to close S1.

A replicated virtual abdomen is also synthesized using Matlab 2020a to reassemble the augmented reality training scenario with a realization of the physical interface location relative to the human abdominal anatomy. As shown in Fig. 1, the virtual abdomen phantom is divided into nine regions

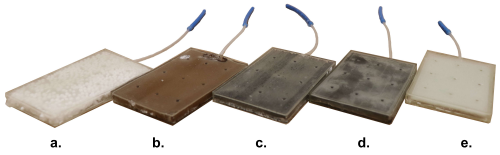

Fig. 4. The five designs for the tunable stiffness muscle layer: **(a)** soft granular jamming made from polystyrene (diameter of 1-2.5 mm), **(b)** fine granular jamming made from ground coffee, **(c)** rigid granular jamming with glass beads (diameter of 1̃ mm), **(d)** stretchable layer jamming with latex membrane (thickness of 0.25mm), and **(e)** non-stretchable layer jamming with matte surfaced polyethylene terephthalate film (Mylar) (thickness of 0.18mm).

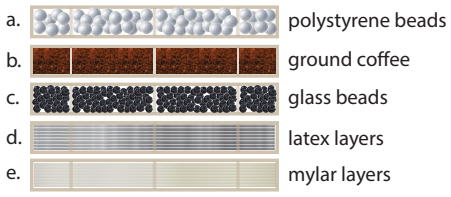

Fig. 5. The cross-section view of the five designs: **(a)** soft granular jamming, **(b)** fine granular jamming, **(c)** rigid granular jamming, **(d)** stretchable layer jamming, and **(e)** non-stretchable layer jamming.

across the four quadrants to describe regional anatomy followed by standard clinical protocol [1]. The position of the haptic mouse is mapped to the position of the virtual pointer (indicated by the organ square) displayed on the phantom. During training, the user is able to set up one or more regions in the virtual phantom as painful regions. The virtual face avatar and the facial expressions are generated through MakeHuman with a simplified binary approach to indicate pain or not pain [20].

III. Design and Fabrication of the Tunable Stiffness Muscle Layer

Five thin-layer samples with different media were designed and fabricated as tunable muscle layers, see Fig. 4. The samples can be easily embedded in the composition of manikin phantoms underneath the skin and subcutaneous fat. We designed the tunable stiffness muscle as a thin flat sheet (80mm length and 50mm width) with an overall thickness of 8mm to simulate the rectus abdominis muscle along the front of the abdomen. Stiffening technologies with granular jamming and layer jamming were selected to achieve the flexibility and softness of a natural muscle [21]. The 1 mm thickness external membrane for the muscle layer was 3D printed with Agilus on a Stratasys CONNEX3 OBJET500 printer. Considering that granule materials are facing the challenge of material rearrangement and distribution, small soft pins with a diameter of 1.2mm were designed to connect the top and bottom surface of the membrane and fix the granule in place. Fig. 5 shows detailed schematics of the 3D printed samples. Vacuum tubes and filters were added to the end side of the samples. The cavity volume is the same as 19.54 $cm^3$for all the non-pressurized samples.

A. Granular jamming with soft, rigid and fine granules

Based on our previous work on granular materials and dimensions for jamming performance [21], three different types of granular fillings were implemented in the muscle layer design as soft granules, fine granules, and rigid granules. Soft granules that allow the deformation of the material can result in high volume shrinkage and tight packing during the activation [22]. Polystyrene beads with diameters between 1.5 to 3mm were used in the study as the soft granules. The design implementation schematics are shown in Fig. 5a. Ground coffee was chosen as the fine granule type filling in the study (Fig. 5b). Research has indicated that it has the advantage of a high strength-to-weight ratio, stiffness-to-density, and yield stress [23]. 1mm diameter matt-surfaced glass beads were employed in the muscle layer to evaluate rigid granular jamming with a larger size, see Fig. 5c. All types of granules were filled in the 3D printed soft cavities with ease and sealed properly to ensure the airtightness of the system. The samples' weight is 11g, 24g, and 16g for the soft granule, rigid granule, and fine granule, respectively.

B. Layer jamming with stretchable and non-stretchable layers

Layer jamming structures were also explored in the muscle layer's design with the comparison between stretchable material and non-stretchable material. Latex sheets with a thickness of 0.25mm were chosen to enable the stretchable layer jamming. Twelve layers of the thin sheet latex were stacked together and fixed through the previously mentioned soft pins to keep them in the desired location within the 3D printed envelope. The schematic is shown in Fig. 5 d. Similarly, laser-cut thin layers of Mylar sheet with a thickness of 0.18mm were used to represent the non-stretchable layer jamming. The implementation of the Mylar sheet is the same as the latex sheet (Fig. 5 e.). The samples' weight is 17g and 15g for the stretchable and non-stretchable layer jamming samples, respectively.

IV. Experimental Characterization

A. Test 1: Simulated stiffness

Fig. 6 shows the indentation test setup used to characterize the ex-vivo porcine samples and fabricated muscle samples. The 3D printed probe is mounted on a 3 axis Cartesian robot, composing of an Aerotech ANT130 XY-stage (Aerotech Inc., resolution of 1nm) for planar movement and an Actuonix linear actuator (L12-30-50-6-I) for vertical indentation in the z-direction. The probe has a spherical tip with the radius $r_p = 10$ mm to ensure the safety of the samples as sharp edges of a flat-tipped probe may tear the samples. An ATI Mini40 force/torque sensor was attached to the probe to measure the indentation force data, F_z. The samples are placed underneath the probe with the air channel connected to a vacuum pump with a pressure regulator (BACOENG 220 V/50 Hz BA-1 Standard). A National Instruments PCIe-6320 is used to acquire the force/torque sensor signals while the linear actuator position is measured and controlled with a

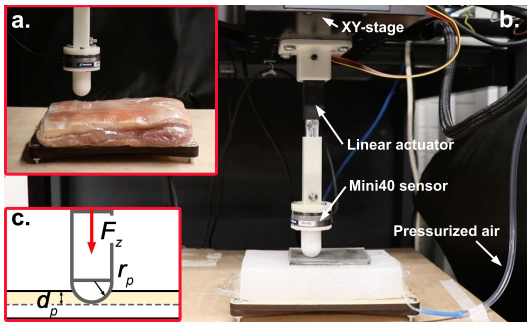

Fig. 6. Indentation test to evaluate the sample stiffness. **(a)** Test on the ex-vivo porcine belly. **(b)** Test on the artificial muscle layer. **(c)** The schematic diagram for the probe contact model.

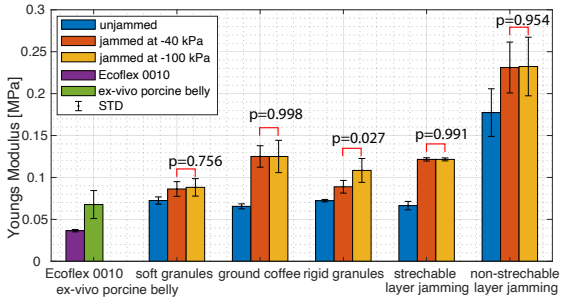

Fig. 7. Characterized stiffness of the Ecoflex 0010 sample, ex-vivo porcine belly, and five artificial muscle samples in unjammed, -40kPa jammed, and -100kPa jammed states. Mean value and standard deviation data from 5 repeated trials are shown.

National Instruments USB-6341 DAQ. The programs to run the experiment and to collect the data have been implemented using Labview 2018.

The experiments were conducted on an ex-vivo porcine belly, an Ecoflex 0010 sample, and an Ecoflex 0010 with an additional layer of tunable stiffness muscle. More specifically, the experiments were conducted on the five different samples from non-jamming states to jamming states actuated at the vacuum level of 0, -40, and -100 kPa. The vacuum pressure levels were chosen with the consideration that the small vacuum pump used in the haptic mouse setup (Section. II) can generate a pressure of around -40 kPa for the tunable stiffness muscle sample under the rated voltage of 12v. The experiment was started by positioning the XY-stage in the center of the sample, with the probe in the initial position (tangent to the surface). The linear actuator was then employed to perform sequential indentation with a step increment equal to 2mm (up to $\sim$ 16mm). For each step performed, the data from the force sensor was recorded in correlation with the displacement. All experiments were repeated five trials while the Cartesian robot moves the probe to different testing locations across the trials.

The lumped stiffness of the samples were evaluated with the steady-state stress σ and strain ε data after the relaxation. We define the lumped stiffness E as $\frac{\sigma}{\varepsilon}$, and $\sigma = \frac{F}{A}$, $\varepsilon = \frac{\Delta L}{L_0}$, where F is the measured force, A is the contact area, ΔL is the indentation displacement, and L_0 is the original width of the sample. Since the probe end is spherical, the contact area A is computed for two regions. When the probing depth $d_p < r_p$, $A = \pi(2r_p d_p - d_p^2)$, while when $d_p > r_p$, $A = \pi r_p^2$ (see Fig. 6 c). Thus, the stiffness is determined by the linear approximation represented by the slope of the stress and strain.

Fig. 7 reports the stiffness change before and after the jamming effect for the five artificial samples in comparison to the porcine belly sample and the Ecoflex 0010 sample. During the non-jamming conditions, samples made of soft granules, rigid granules, and fine granules (ground coffee), as well as the stretchable layer jamming sample, show closer stiffness to the porcine belly sample. However, the non-stretchable layer jamming sample made of mylar shows significantly higher stiffness compared to the rest.

An increase in stiffness can be observed in all five samples, with the ground coffee granular jamming and stretchable layer jamming shows the largest increase. The stiffness change during the jamming is relatively small for the soft granules under the same volume condition compare to the other media. At the pressure level of -40 kPa, most artificial samples already reach their maximum simulated stiffness, while only the rigid granular sample made of glass beads still increases when being jammed at -100 kPa. A student t-test was carried out to compare the statistical difference between the stiffness generated with pressure at -40 and -100 kPa. The p-values are stated in Fig. 7. This result shows that the use of a small vacuum pump to generate around -40 kPa pressure is applicable for the given application.

B. Test 2: Response time of the tunable stiffness mechanism

Muscle guarding is an effective self-protection mechanism that works on fast reflexes. The transition time was measured as the stabilized time taken to reach the maximum jamming pressure of around -40kPa with a pressure sensor and the activation of the vacuum pump. The pressure data were recorded at 1k Hz and analyzed with the rate of pressure change, shown in Fig. 8a and c, respectively. The rate of pressure change is computed by taking the derivative of the pressure data with respect to time. The test was performed five times to compute the mean value and standard deviation. The experiment shows very good repeatability, where the standard deviations are relatively small. The enlarged view of the pressure response during the jamming state transit is shown in Fig. 8b and d, where the standard deviation is represented with shaded error bars.

The result is shown in Table I with comparisons in the sample's weight, density, and increased stiffness after activation (at -40kPa). The densities of the samples were computed with the measured volume and weight of each sample. The fine granule (ground coffee) sample shows the highest stiffness increase to weight ratio at 0.0037 MPa/g, followed by the non-stretchable layer jamming sample at 0.0036 MPa/g. It can be observed that most of the samples have an activation time of around 1 to 2 seconds on average, with the rigid granular jamming sample made of glass beads showing the longest time in activation around 1.96s. The

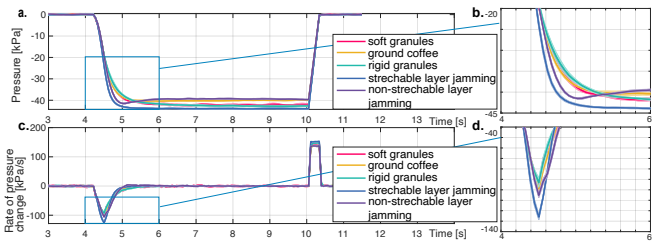

Fig. 8. **(a)** Pressure response during the jamming activation for all the five samples. **(b)** Enlarged view of the pressure response during the transit state. **(c)** Rate of pressure change during the jamming activation for all the five samples. **(d)** Enlarged view of the rate of pressure change during the transit state. All data are reported with the mean value of 5 trials of experiments. The standard deviation is reported by giving the shaded error bar of the same color.

TABLE I

PHANTOM CHARACTERISTICS

Phantom types	Material	Weight (g)	Density (g/cm^3)	Increased stiffness (MPa)	Activation time mean (STD) (s)
Soft granule	Polystyrene beads	11	0.56	0.0137	1.22 (0.24)
Fine granule	Ground coffee	16	0.82	0.0595	1.32 (0.15)
Rigid granule	Glass beads	24	1.23	0.0166	1.96 (0.41)
Stretchable layer	Thin latex	17	0.87	0.0552	1.19 (0.16)
Non-stretchable layer	Mylar	15	0.77	0.0537	0.89 (0.03)

layer jamming approach, in general, shows faster activation time than the granular jamming approach. The quickest activation time is for non-stretchable layer jamming made of Mylar, which is around 0.89s.

V. USER STUDY ON MUSCLE GUARDING

User tests of manual palpation were then performed to test the usability of the proposed simulation mechanisms in representing muscle guarding. 10 healthy naive subjects with no hand/wrist injury were recruited in the experiment. The subjects are within the age group of 24-49 years old (n = 10, 2 females, 8 males, M = 32.4, SD = 7) and have no experience in medical palpation. All the subjects are right-handed, with the handedness score between 55-100 (M = 80, SD = 19.72) according to the pre-taken handedness test [24]. The experimental protocol was approved by Imperial College London Sciences Engineering Technology Research Ethics Committee (Protocol number 20IC5867).

During the user test (Fig. 9), subjects were asked to sit in a relaxed posture in front of the phantom placed on a lab desk. The subjects were then asked to use their dominant hand to perform the palpation examinations direct on the top of the phantom. During the experiment, the subjects wore eye-masks so as not to obtain cues from sight. The observer guided each subject's hand to the place of the phantom. An ATI mini40 force and torque sensor were placed underneath

TABLE II

USER STUDY PROTOCOL

Transfer of knowledge	Providing the clinical context: Subjects were asked to read descriptions of abdominal palpation, muscle guarding, and abdominal rigidity.	
	A clip of clinical abdominal palpation training was provided for the subject to watch.	
User test	Training phase	Subjects received stimuli from known apparatuses S-a (activated jamming) and S-n (non-activated jamming), successively, and memorized the feelings. Within each trial, the subject has 10 seconds to remember the feeling. 8 training trials were provided for each sample with each subject. The state of the phantom S-a and S-n are sampled one after another during the training.
	Testing phase	Subjects were then provided with a phantom with a randomized unknown apparatus and asked to diagnose it as either S-a or S-n. The subject's examination time is not constrained. 10 trials tests were performed for each sample with each subject. The correctness rate was recorded.
	The training and testing phase were then repeated for the five different phantoms.	

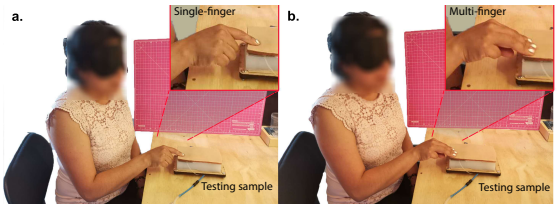

Fig. 9. User test: evaluating if the sample is stiffen or relax with **(a)** single finger palpation and **(b)** multi-finger palpation

the phantom to collect the palpation force data. Two types of tests were performed with the five samples according to the palpation hand gesture. During the first test, subjects were asked to palpate with only a single finger (index finger). In the second test, subjects were asked to palpate with multiple fingers (index finger, middle finger, and ring finger). Two states were simulated with each sample (S-a and S-n), where S-a is when the muscle layer is actuated to simulate abdominal guarding, and S-n is when the muscle layer is deactivated at their relaxed state. The actuation's audible effect is altered to ensure the participants cannot differentiate the simulation types by sound. The detailed user test protocol is shown in Table II.

The result of the correctness rate in the user test is shown in Fig. 10 a. On each box, the central mark indicates the median, while the bottom and top edges of the box indicate the 25% and 75% of the data, respectively. The accuracy for diagnosing the soft granule sample is the lowest among the five. This is in alignment with the previous material characterization in Section. IV-A, where the soft granule based granular jamming also exhibits the lowest stiffness change during the actuation. The single finger palpation shows higher accuracy in examining the ground coffee-based granular jamming sample compared to using multi-finger pal-

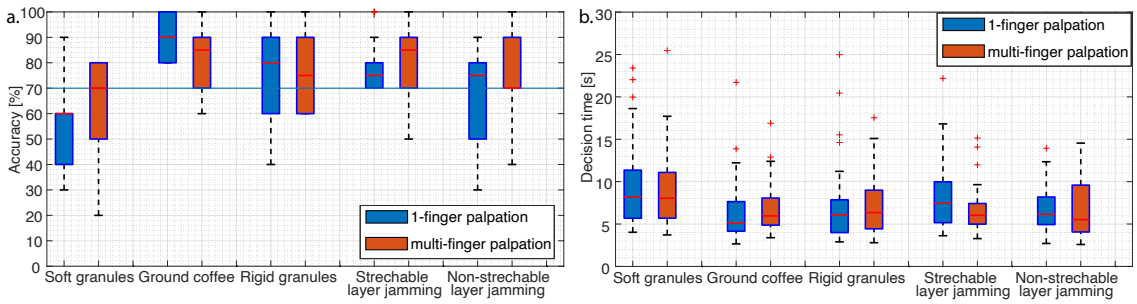

Fig. 10. **(a)** The decision correctness rate of the user tests in percentage (%). The blue line indicates the 70% of decision-making accuracy. **(b)** The time taken to make the decision during the user tests. The median, the 25%, and 75% of the data are shown with the box plot, while the whiskers extend to the most extreme data points (not considered outliers). The "+" symbols indicate the outliers. The blue line in indicates the 70% of decision making accuracy.

pation. Although the stretchable layer jamming sample shows similar simulated stiffness compared to the ground coffee sample, the detection accuracy shows a higher success rate with multi-finger palpation. This interesting result can also be observed in the granular jamming sample made of rigid granules and the non-stretchable layer jamming sample. As we know from previous research, layer jamming mechanisms generate higher shear stiffness compare to granular jamming mechanisms [25]. Palpation with multiple fingers could be more effective in detecting the haptic difference in the shear directions. This could be a cue to indicate optimal palpation gesture is depending on the given haptic stimuli. If only detecting the stiffness of a particular region, naive subjects show no advantages in using multiple fingers. Furthermore, the time taken for making the decision during the testing phase was calculated by analyzing the force profile. Fig. 10 b shows the decision-making time for the five types of samples for the 10 subjects. The decision-making time shows a very similar trend to the decision accuracy. In general, the longer the subjects took to make the decision, the lower accuracy they achieved.

The usability of the samples in simulating tunable stiffness abdominal muscle was further evaluated by placing a threshold of 70% in the decision accuracy (Fig. 10 a). Higher accuracy in both single-finger and multiple-finger palpation user tests indicates that a more evident sign of muscle guarding was presented and detected with the specified sample. The samples made of ground coffee and stretchable layers show the highest detection rate among the five samples, while at least 75% of the user data exhibits more than 70% of decision accuracy.

VI. Discussion and Conclusion

In this paper, we proposed and experimentally characterized five different jamming mechanisms in representing tunable stiffness muscle. Granular jamming structures with soft, fine, and rigid granules were tested in comparison to layer jamming structures with stretchable and non-stretchable layers. All samples show a similar stiffness range compared to the ex-vivo porcine belly sample, while the non-stretchable layer jamming mechanism shows the highest absolute stiffness, and the soft granule mechanism shows the smallest stiffness change among all five samples. A simplified linear model was used in this paper to evaluate the sample material property after the stress relaxation for reduced parameters and simplifications of comparison. Stress relaxations were observed in the indentation test across all fabricated samples and the ex-vivo porcine belly sample, while future studies will be carried on nonlinear tissue modeling and characterization of specific materials to further enhance the haptic surface rendering fidelity. In the user test, all users agree that the machine simulates a realistic feeling of the human abdomen. Tests with different gestures of single-finger and multi-finger palpation demonstrate the adaptability of the proposed haptic rendering mechanism in different interaction contexts. The ground coffee granular jamming sample shows the highest detection accuracy and least decision time for the single-finger palpation. The stretchable layer jamming sample shows the highest detection accuracy in multi-finger palpation tests with the smallest variance in the decision time across all subjects. Granular jamming made of ground coffee can simulate clear stiffness change in rendering biological tissue for palpation training. However, the method experiences significant variance in large area simulation due to the rearrangement of the granules. Stretchable latex for layer jamming also shows promising results in stiffness rendering and has less limitation in simulating larger and curve-surfaced structures.

Current virtual training is limited by the available quantitative clinical data of patients with different physiological conditions. In future studies, clinical studies will be conducted with specially designed sensors to measure live human subjects' abdomen stiffness change [26]. The measurement will be used to create a data set with correlated physiological and pathological information of the patient. The data set can then be processed to the training environment where the simulated stiffness is programmed to match the real patient conditions. The long-term performance of the system is also considered for future studies.

Acknowledgment

The authors would like to thank Jacob Tan for his help in rendering the facial images and Jacob Mitchell for his help in acquiring the ex-vivo porcine samples.

REFERENCES

[1] L. Bickley and P. G. Szilagyi, *Bates' guide to physical examination and history-taking*. Lippincott Williams & Wilkins, 2012.

[2] C. Ferguson, "Inspection, auscultation, palpation, and percussion of the abdomen," *Clinical Methods: The History, Physical, and Laboratory Examinations: 3rd edition*, pp. 473–477, 1990.

[3] C. Jarvis, *Physical examination & health assessment*, 7th ed. Elsevier B.V., 2015.

[4] Y. Zhang, R. Phillips, J. Ward, and S. Pisharody, "A survey of simulators for palpation training," *Studies in health technology and informatics, 142*, pp. 444–446, 2009.

[5] C. M. Ferguson, "Inspection, auscultation, palpation, and percussion of the abdomen," *Clinical Methods: The History, Physical and Laboratory Examinations. 3rd edn. Boston, MA: Butterworths*, 1990.

[6] T. D. Lalitharatne, Y. Tan, F. Leong, L. He, N. Van Zalk, S. De Lusignan, F. Iida, and T. Nanayakkara, "Facial expression rendering in medical training simulators: Current status and future directions," *IEEE Access*, vol. 8, pp. 215 874–215 891, 2020.

[7] M. L. Ribeiro, H. M. Lederman, S. Elias, and F. L. Nunes, "Techniques and devices used in palpation simulation with haptic feedback," *ACM Computing Surveys (CSUR)*, vol. 49, no. 3, pp. 1–28, 2016.

[8] S. Ramani, "Twelve tips for excellent physical examination teaching," *Medical Teacher*, vol. 30, no. 9-10, pp. 851–856, 2008.

[9] C. R. Macaluso and R. M. McNamara, "Evaluation and management of acute abdominal pain in the emergency department," *International journal of general medicine*, vol. 5, p. 789, 2012.

[10] E. P. Scilingo, M. Bianchi, G. Grioli, and A. Bicchi, "Rendering softness: Integration of kinesthetic and cutaneous information in a haptic device," *IEEE Transactions on Haptics*, vol. 3, no. 2, pp. 109–118, 2010.

[11] T. R. Coles, D. Meglan, and N. W. John, "The role of haptics in medical training simulators: a survey of the state of the art," *IEEE Transactions on haptics*, vol. 4, no. 1, pp. 51–66, 2010.

[12] M. Manti, V. Cacucciolo, and M. Cianchetti, "Stiffening in soft robotics: A review of the state of the art," *IEEE Robotics & Automation Magazine*, vol. 23, no. 3, pp. 93–106, 2016.

[13] K. B. Shimoga, "A survey of perceptual feedback issues in dexterous telemanipulation. ii. finger touch feedback," in *Proceedings of IEEE Virtual Reality Annual International Symposium*, 1993, pp. 271–279.

[14] "Touch (haptic device, 3d systems)," Jun 2020. [Online]. Available: https://uk.3dsystems.com/haptics-devices/touch

[15] M. Li, T. Ranzani, S. Sareh, L. D. Seneviratne, P. Dasgupta, H. A. Wurdemann, and K. Althoefer, "Multi-fingered haptic palpation utilizing granular jamming stiffness feedback actuators," *Smart Materials and Structures*, vol. 23, no. 9, p. 095007, 2014.

[16] A. A. Stanley and A. M. Okamura, "Controllable Surface Haptics via Particle Jamming and Pneumatics," *IEEE Transactions on Haptics*, vol. 8, no. 1, pp. 20–30, 2015.

[17] L. He, N. Herzig, S. de Lusignan, and T. Nanayakkara, "Granular jamming based controllable organ design for abdominal palpation," in *2018 40th Annual International Conference of the IEEE Engineering in Medicine and Biology Society (EMBC)*, July 2018, pp. 2154–2157.

[18] L. He, N. Herzig, S. d. Lusignan, L. Scimeca, P. Maiolino, F. Iida, and T. Nanayakkara, "An abdominal phantom with tunable stiffness nodules and force sensing capability for palpation training," *IEEE Transactions on Robotics*, pp. 1–14, 2020.

[19] M. Koehler, N. S. Usevitch, and A. M. Okamura, "Model-based design of a soft 3-d haptic shape display," *IEEE Transactions on Robotics*, vol. 36, no. 3, pp. 613–628, 2020.

[20] T. D. Lalitharatne, Y. Tan, L. He, F. Leong, N. Van Zalk, S. de Lusignan, F. Iida, and T. Nanayakkara, "Morphface: A hybrid morphable face for a robopatient," *IEEE Robotics and Automation Letters*, vol. 6, no. 2, pp. 643–650, 2021.

[21] A. Jiang, T. Ranzani, G. Gerboni, L. Lekstutyte, K. Althoefer, P. Dasgupta, and T. Nanayakkara, "Robotic granular jamming: Does the membrane matter?" *Soft Robotics*, vol. 1, no. 3, pp. 192–201, 2014.

[22] A. B. Clark and N. Rojas, "Assessing the performance of variable stiffness continuum structures of large diameter," *IEEE Robotics and Automation Letters*, vol. 4, no. 3, pp. 2455–2462, 2019.

[23] N. G. Cheng, "Design and analysis of jammable granular systems," Ph.D. dissertation, Massachusetts Institute of Technology, 2013.

[24] R. C. Oldfield *et al.*, "The assessment and analysis of handedness: the edinburgh inventory," *Neuropsychologia*, vol. 9, no. 1, pp. 97–113, 1971.

[25] S. G. Fitzgerald, G. W. Delaney, and D. Howard, "A review of jamming actuation in soft robotics," *Actuators*, vol. 9, no. 4, p. 104, 2020.

[26] N. Herzig, L. He, P. Maiolino, S.-A. Abad, and T. Nanayakkara, "Conditioned haptic perception for 3d localization of nodules in soft tissue palpation with a variable stiffness probe," *PLOS ONE*, vol. 15, no. 8, pp. 1–31, 08 2020. [Online]. Available: https://doi.org/10.1371/journal.pone.0237379